

# Secondary instabilities of hexagons: a bifurcation analysis of experimentally observed Faraday wave patterns

A.M. Rucklidge, M. Silber, and J. Fineberg

**Abstract.** We examine three experimental observations of Faraday waves generated by two-frequency forcing, in which a primary hexagonal pattern becomes unstable to three different superlattice patterns. We use the symmetry-based approach developed by Tse *et al.* [1] to analyse the bifurcations involved in creating the three new patterns. Each of the three examples reveals a different situation that can arise in the theoretical analysis.

## 1. Introduction

The classic Faraday wave experiment consists of a horizontal layer of fluid that spontaneously develops a pattern of standing waves on its surface as it is driven by vertical oscillation with amplitude exceeding a critical value. Recent experiments have revealed a wide variety of complex patterns, particularly in the large aspect ratio regime and with a forcing function containing two commensurate frequencies [2, 3, 4]. Transitions from the flat surface to a primary, spatially periodic, pattern can be studied using equivariant bifurcation theory [5]. These group theoretic techniques may also be applied to secondary spatial period-multiplying transitions to patterns with two distinct spatial scales (so called *superlattice* patterns) as demonstrated by Tse *et al.* [1].

We apply the method of Tse *et al.* [1] to the analysis of three superlattice patterns observed when secondary subharmonic instabilities destroy the basic hexagonal standing wave pattern in two-frequency Faraday wave experiments. We can make use not only of the general symmetry-based approach from [1] but also of many of the detailed results. The reason for this is that in their paper, Tse *et al.* considered instabilities of hexagonal patterns that broke the translation symmetry of the hexagons, but that remained periodic in a larger hexagonal domain comprising twelve of the original hexagons. The instabilities under consideration here satisfy exactly the same conditions (though in fact they remain periodic in smaller domains as well).

We begin by specifying the coordinate system and symmetries we will use in section 2, then describe the symmetries of the three experimental patterns in

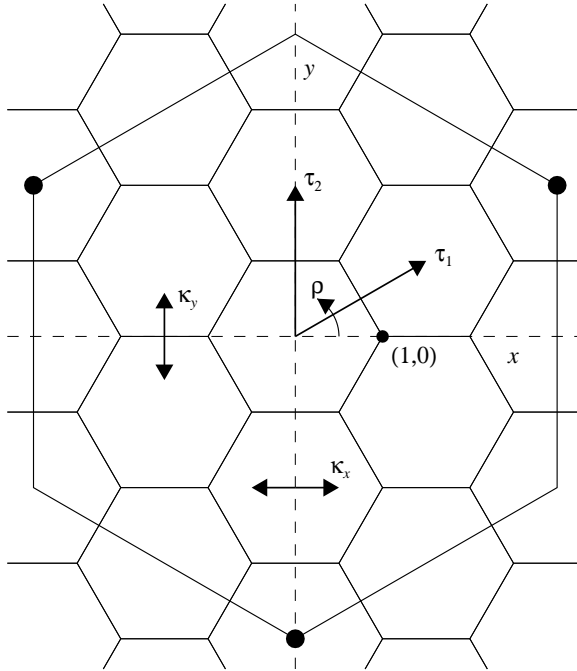


FIGURE 1. The coordinate system and certain elements of the symmetry group  $\Gamma$ . The origin of the coordinate system is at the centre of the diagram, and the point  $(1, 0)$  is indicated. The small hexagons represent the primary pattern, which is invariant under reflections ( $\kappa_x$  and  $\kappa_y$ ),  $60^\circ$  rotations ( $\rho$ ) and translations ( $\tau_1$  and  $\tau_2$ ). The secondary patterns are all periodic in the larger hexagonal box. The three corner points labelled with solid circles are identified through the assumed periodicity.

section 3. In section 4, we apply Tse *et al.*'s method of analysis to these three patterns, and present normal forms and stability calculations in section 5. We conclude in section 6.

## 2. Coordinates and symmetries

The primary pattern is made up of regular hexagons, which are invariant under the group  $D_6$  (made up of  $60^\circ$  rotations and reflections) combined with translation from one hexagon to the next (see figure 1). Tse *et al.* [1] studied experimental patterns reported in [6], which had the feature that after the secondary instability,

the pattern remained periodic in the larger hexagonal box in figure 1. The 144-element spatial symmetry group of the primary hexagonal pattern within this box is  $\Gamma$ , generated by the following reflection  $\kappa_x$ , rotation  $\rho$  and translations  $\tau_1$  and  $\tau_2$ :

$$\kappa_x : (x, y) \rightarrow (-x, y) \qquad \tau_1 : (x, y) \rightarrow (x, y) + \left( \frac{3}{2}, \frac{\sqrt{3}}{2} \right) \quad (1)$$

$$\rho : (x, y) \rightarrow \left( \frac{1}{2}x - \frac{\sqrt{3}}{2}y, \frac{\sqrt{3}}{2}x + \frac{1}{2}y \right) \qquad \tau_2 : (x, y) \rightarrow (x, y) + (0, \sqrt{3}) \quad (2)$$

We also define  $\kappa_y = \kappa_x \rho^3$ , and note the following identities:

$$\kappa_x^2 = \kappa_y^2 = \rho^6 = \tau_1^6 = \tau_2^6 = \tau_1^2 \tau_2^2 = \text{identity}, \quad (3)$$

$$\rho \kappa_x = \kappa_x \rho^5, \quad \tau_1 \kappa_x = \kappa_x \tau_1^5 \tau_2, \quad \tau_2 \kappa_x = \kappa_x \tau_2, \quad (4)$$

$$\tau_1 \rho = \rho \tau_1^3 \tau_2, \quad \tau_2 \rho = \rho \tau_1, \quad \tau_1 \tau_2 = \tau_2 \tau_1. \quad (5)$$

The time translation  $\tau_T$  advances time by one period  $T$  of the forcing function, which is the same as the temporal period of the hexagonal pattern. This time translation is combined with the spatial symmetries above to give spatio-temporal symmetries.

### 3. Experimental patterns

The three experimentally observed patterns are shown in figure 2(a-c), visualised using the techniques described in [7]. Patterns (a) and (b) are both obtained using Dow-Corning silicone oil with viscosity 47 cSt and layer depth 0.35 cm, while pattern (c) was found using a 23 cSt oil layer of depth 0.155 cm. All three patterns are obtained with forcing function containing two frequencies in the ratio 2 : 3; pattern (a) is found with frequencies 50 and 75 Hz, pattern (b) with frequencies 70 and 105 Hz, and pattern (c) with 40 and 60 Hz driving frequencies. Pattern (c) was reported previously in [7]. Typically, the secondary bifurcations occur at forcing amplitudes between 10 and 50% larger than the critical acceleration for the primary hexagonal state. Further experimental details can be found in [7, 8].

For the purposes of the analysis, we consider the idealised versions of these experimental patterns, shown in figure 2(d-f). The first pattern in figure 2(a,d) retains the  $D_6$  symmetry of the original hexagons but breaks certain translation symmetries. It is periodic in the medium-sized dashed hexagon in figure 2(d), which implies that the pattern is invariant under the translations  $\tau_1^3$  and  $\tau_1 \tau_2$ . It has no spatio-temporal symmetries. The second pattern is similar, although it possesses only triangular ( $D_3$ ) symmetry instantaneously. Moreover, it has the spatio-temporal symmetry given by a  $60^\circ$  rotation combined with advance in time by one period  $T$  of the forcing, as in figure 2(e,g). In fact, this spatio-temporal symmetry was first suggested by the analysis below, and found to be consistent with the experimental observations. The third pattern in figure 2(c,f) is quite different: the dark lozenges in figure 2(f) represent the enlarged gaps between

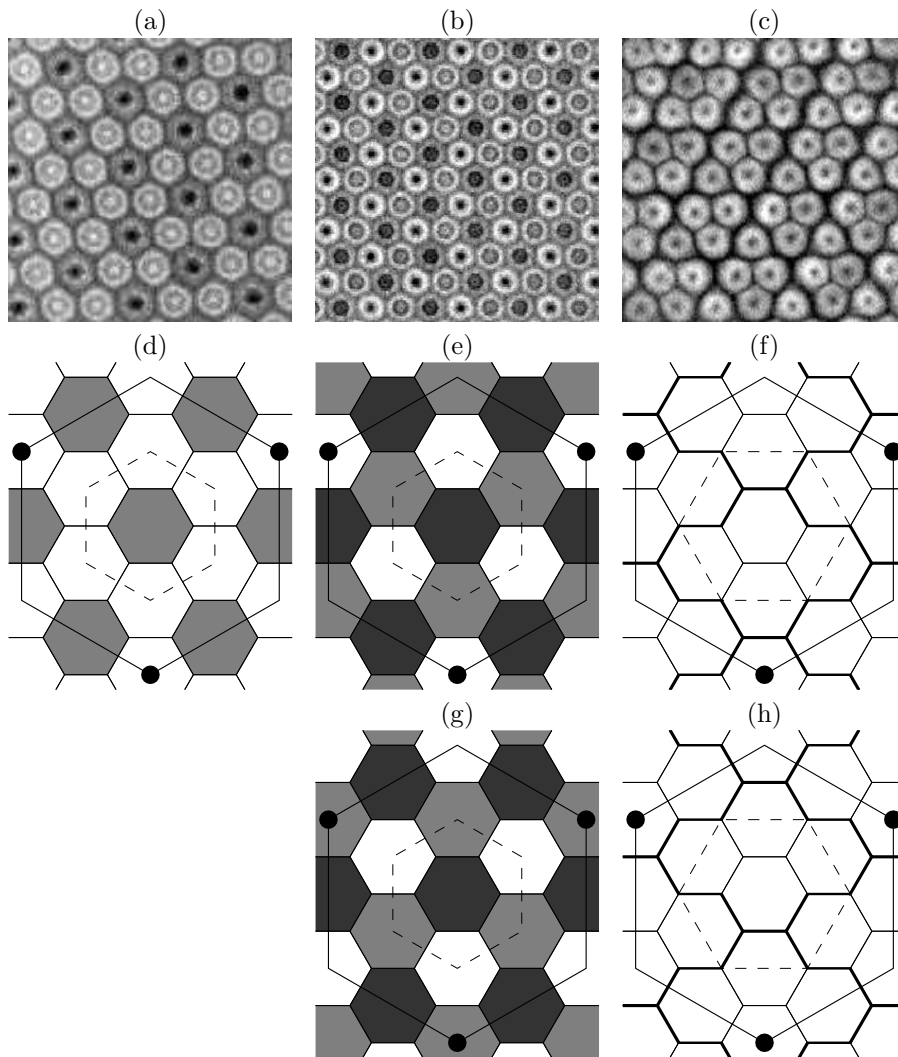


FIGURE 2. Experimental and idealised secondary patterns. (a-c) Experimental patterns, visualised from above. (d-f) Idealised versions of (a-c). (g-h) patterns (e-f) but seen one forcing period  $T$  later. The idealisations are all rotated by about  $30^\circ$  compared with the experimental pictures.

	a	b	c	d	e	f	g	h	i	j	k	l	m	n	o
id	$\kappa_x$	$\kappa_y$	$\tau_1$	$\tau_1^2$	$\tau_1^3$	$\kappa_x\tau_1$	$\kappa_x\tau_2$	$\kappa_x\tau_1^3$	$\kappa_y\tau_1^3$	$\rho$	$\rho^2$	$\rho^3$	$\rho^2\tau_1$	$\rho^3\tau_1^3$	
1	6	18	6	2	3	12	12	6	18	24	8	3	16	9	
1	1	1	1	1	1	1	1	1	1	1	1	1	1	1	1
2	1	-1	-1	1	1	1	-1	-1	-1	1	1	1	1	1	1
3	1	1	-1	1	1	1	1	1	1	-1	-1	1	-1	1	-1
4	1	-1	1	1	1	1	-1	-1	-1	1	-1	1	-1	1	-1
5	2	0	0	2	2	2	0	0	0	0	1	-1	-2	-1	-2
6	2	0	0	2	2	2	0	0	0	0	-1	-1	2	-1	2
7	2	2	0	-1	-1	2	-1	-1	2	0	0	2	0	-1	0
8	2	-2	0	-1	-1	2	1	1	-2	0	0	2	0	-1	0
9	3	1	1	-1	3	-1	-1	1	-1	-1	0	0	3	0	-1
10	3	-1	1	-1	3	-1	1	-1	1	-1	0	0	-3	0	1
11	3	-1	-1	-1	3	-1	1	-1	1	1	0	0	3	0	-1
12	3	1	-1	-1	3	-1	-1	1	-1	1	0	0	-3	0	1
13	4	0	0	-2	-2	4	0	0	0	0	0	-2	0	1	0
14	6	-2	0	1	-3	-2	-1	1	2	0	0	0	0	0	0
15	6	2	0	1	-3	-2	1	-1	-2	0	0	0	0	0	0

TABLE 1. Character table of the group  $\Gamma$ , taken from Tse *et al.*, with corrections. A representative element is shown on the second line for each conjugacy class (see also figure 3), and the number of elements in the class is on the third row. The next fifteen rows give the characters associated with each conjugacy class for each of the fifteen representations.

the hexagons in figure 2(c). The pattern is periodic in the medium-sized dashed hexagon in figure 2(f), so is invariant under translations  $\tau_1^2$  and  $\tau_2^2 = \tau_1^4$ . It is also invariant under the group of symmetries of a rectangle  $D_2$ , and possesses the spatio-temporal symmetry of the translation  $\tau_2$  combined with advance in time by one period  $T$  of the forcing, as in figure 2(f,h).

Using the information above, we write down the instantaneous (spatial) symmetry groups of the three patterns from figure 2(a-c) in terms of their generators:

$$\Sigma_a = \langle \kappa_x, \rho, \tau_1^3, \tau_1\tau_2 \rangle, \quad \Sigma_b = \langle \kappa_x, \rho^2, \tau_1^3, \tau_1\tau_2 \rangle, \quad \Sigma_c = \langle \kappa_x, \kappa_y\tau_2, \tau_1^2 \rangle. \quad (6)$$

These groups are of order 48, 24 and 12 respectively. For the full spatio-temporal symmetry groups, we would also include  $\rho\tau_T$  in the generators of  $\Sigma_b$ , and  $\tau_2\tau_T$  in the generators of  $\Sigma_c$ , but initially we will work with the spatial symmetry groups. The reason for this is that the instantaneous (spatial) symmetries can be determined reliably from a single experimental image, while extracting spatio-temporal symmetries from the experimental data is more involved.

Each of the three instabilities that generates the three different patterns will be associated with a set of marginally stable eigenfunctions; the new pattern, at least near onset, can be thought of as (approximately) a linear combination of

these marginal eigenfunctions and the original hexagonal pattern. Which linear superpositions are consistent with the nonlinearity inherent in the pattern formation process is determined by our bifurcation analysis. The symmetries in  $\Gamma$  all leave the primary hexagonal pattern unchanged, so they must send marginal eigenfunctions onto linear combinations of marginal eigenfunctions, which induces an action on the amplitudes of these functions. In other words, if there are  $n$  marginal eigenfunctions  $f_1, \dots, f_n$ , with  $n$  amplitudes  $\mathbf{a} = (a_1, \dots, a_n) \in \mathbb{R}^n$ , each element  $\gamma \in \Gamma$  sends  $\mathbf{a}$  to  $R_\gamma \mathbf{a}$ , where the set of  $n \times n$  orthogonal matrices  $R_\gamma$  forms a representation  $R_\Gamma$  of the group  $\Gamma$ . For subharmonic instabilities of the type of interest here, this will generically be an irreducible representation (irrep) [5]. Tse *et al.* [1] have computed all the irreps of the group  $\Gamma$ ; the character table of these representations is reproduced in table 1. Recall that the character of a group element  $\gamma$  in a representation is the trace of the matrix  $R_\gamma$ , and that conjugate elements (which form a conjugacy class) have the same characters.

Once the representation associated with each of the three transitions is identified, we can write down the normal form, work out what other patterns are created in the same bifurcation, and compute stability of the patterns in terms of the normal form coefficients.

#### 4. Method

The first task is to identify which representation is relevant for each bifurcation. Tse *et al.* [1] outlined a two-stage method to accomplish this. First, any symmetry element that is represented by the identity matrix in a particular representation must appear in the symmetry group of every branch of solutions created in a bifurcation with that representation. This can be used to eliminate from consideration any representation that has an element with character equal to the character of the identity that does not appear in the symmetry group of the observed pattern. Second, we make use of the trace formula from [5], which gives the dimension of the subspace of  $\mathbb{R}^n$  that is fixed by a particular isotropy subgroup  $\Sigma$  of  $\Gamma$  with representation given by the matrices  $R_\Gamma$ :

$$\dim \text{fix}(\Sigma) = \frac{1}{|\Sigma|} \sum_{\sigma \in \Sigma} \text{Tr } R_\sigma, \quad (7)$$

where  $|\Sigma|$  is the number of elements in  $\Sigma$ . Specifically, we use the trace formula to eliminate those representations for which the spatial symmetry group of the pattern fixes a zero-dimensional subspace (implying that the subgroup is not an isotropy subgroup); only the remaining representations need be examined in more detail.

We proceed by first counting the number of elements in each conjugacy class for each of the symmetry groups  $\Sigma_a$ ,  $\Sigma_b$  and  $\Sigma_c$ . Figure 3 shows representative elements from each class and is helpful for this categorization. The result of this

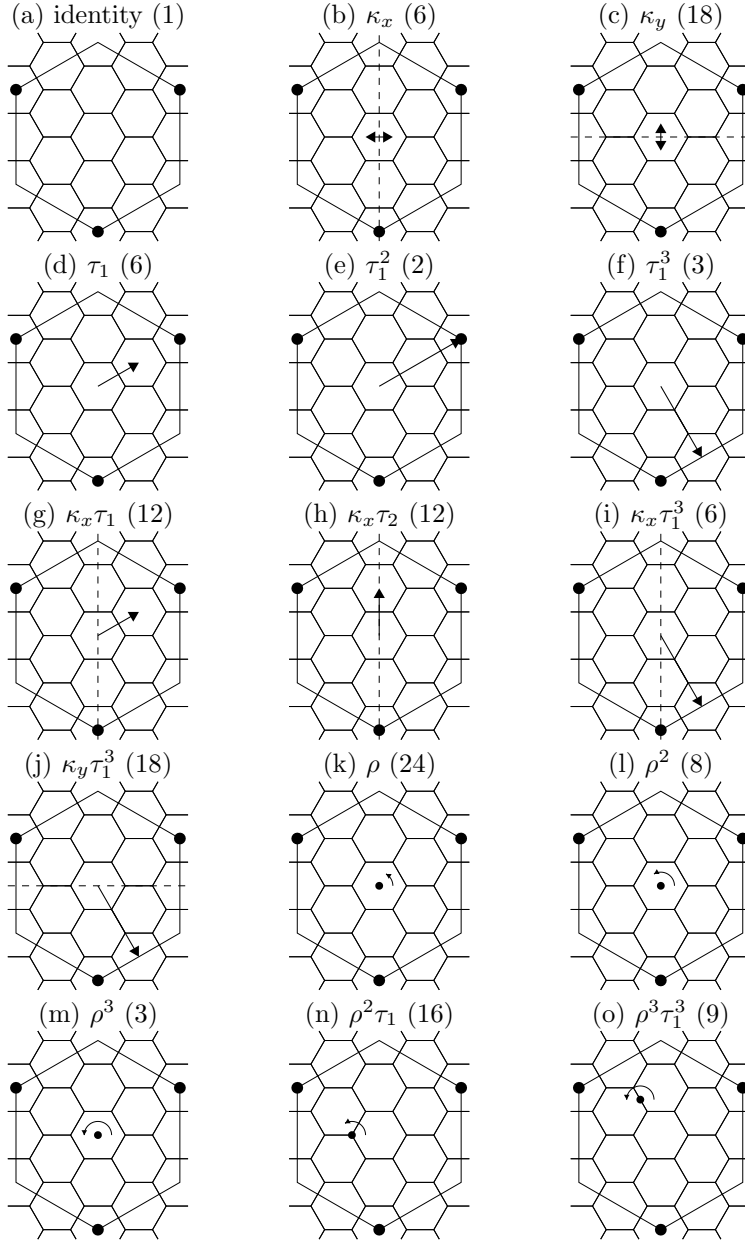


FIGURE 3. The 15 conjugacy classes of  $\Gamma$ . One element from and the number of elements in each class are indicated. The letters (a)–(o) correspond to the columns of table 1.

is:  $\Sigma_a$  contains:

$$a : 1, b : 6, c : 6, f : 3, i : 6, j : 6, k : 8, l : 8, m : 1, o : 3 \quad (8)$$

(that is, one element from class  $a$ , six from class  $b$  etc.);  $\Sigma_b$  contains:

$$a : 1, b : 6, f : 3, i : 6, l : 8; \quad (9)$$

and  $\Sigma_c$  contains:

$$a : 1, b : 1, c : 3, e : 2, h : 2, o : 3. \quad (10)$$

The element  $\tau_1^2$  does not appear in the symmetry groups of patterns (a) and (b), which eliminates representations 1–6 and 9–12 (since  $\tau_1^2$  is represented by the identity matrix in all these: see table 1). Similarly,  $\tau_1\tau_2$  in class  $f$  and  $\rho^3$  do not appear in  $\Sigma_c$ , which eliminates representations 1–9, 11 and 13 from consideration for that bifurcation problem.

Next, by applying (7), we find that pattern (a) has a non-zero dimensional fixed point subspace only in representation 7, as does pattern (b). The spatial symmetry group of pattern (a) fixes a one-dimensional subspace, and that of pattern (b) fixes a two-dimensional subspace. Pattern (c) has a one-dimensional fixed point subspace in representations 10 and 12, and zero in other representations.

We are therefore faced with three different situations: the spatial symmetry group  $\Sigma_a$  fixes a one-dimensional subspace in representation 7, so we expect by the Equivariant Branching Lemma (see [5]) that such a pattern will generically be found in a bifurcation problem with that representation.

Pattern (b), on the other hand, has a spatial symmetry group that fixes a two-dimensional subspace. However, we must take into account that the pattern arises in a subharmonic (period-doubling) instability, and extend the groups  $\Gamma$  and  $\Sigma_b$  to the spatio-temporal symmetry groups that arise by including time translations. We may then show that the spatio-temporal symmetry group of pattern (b) fixes a one-dimensional subspace, and so also arises generically in a subharmonic bifurcation with representation 7. This is the same representation as with pattern (a), obtained for similar experimental parameter values. Extending to include the subharmonic nature of the instability does not affect the branching of pattern (a).

The third situation arises with pattern (c), which on symmetry arguments alone could be associated with either representation 10 or representation 12. Including information about the spatio-temporal symmetry of the pattern does not distinguish between these two representations. However, information on the Fourier transform of the pattern does allow a choice to be made between the two possibilities; in order to show this, we first need to work out which combinations of Fourier modes are associated with each pattern.

It is useful to have sample Fourier modes for the basic hexagonal pattern:

$$f_0(x, y) = \cos 2\pi \left( \frac{2x}{3} \right) + \cos 2\pi \left( -\frac{x}{3} + \frac{y}{\sqrt{3}} \right) + \cos 2\pi \left( -\frac{x}{3} - \frac{y}{\sqrt{3}} \right), \quad (11)$$

with wavevector of length  $\frac{4\pi}{3}$ , as well as sample Fourier modes for representations 7, 10 and 12. The method described by Tse *et al.* [1] yields Fourier functions



that would be included in the eigenfunctions associated with representation 7; representative functions with the shortest wavevectors include:

$$f_1(x, y) = \cos 2\pi \left( \frac{x}{3} + \frac{y}{3\sqrt{3}} \right) + \cos 2\pi \left( \frac{x}{3} - \frac{y}{3\sqrt{3}} \right) + \cos 2\pi \left( \frac{2y}{3\sqrt{3}} \right) \quad (12)$$

$$f_2(x, y) = \sin 2\pi \left( \frac{x}{3} + \frac{y}{3\sqrt{3}} \right) + \sin 2\pi \left( -\frac{x}{3} + \frac{y}{3\sqrt{3}} \right) + \sin 2\pi \left( -\frac{2y}{3\sqrt{3}} \right), \quad (13)$$

which is made up of wavevectors of length equal to  $\frac{1}{\sqrt{3}}$  of that of the basic hexagonal pattern. Eigenfunctions for representation 10 are made up of Fourier functions that include:

$$f_1 = \sin 2\pi \left( \frac{x}{6} + \frac{y}{2\sqrt{3}} \right) \quad f_2 = \sin 2\pi \left( \frac{-x}{6} + \frac{y}{2\sqrt{3}} \right) \quad f_3 = \sin 2\pi \left( \frac{-x}{3} \right), \quad (14)$$

with wavevector of length  $\frac{1}{2}$  the fundamental; and representation 12 has:

$$f_1 = \sin 2\pi \left( \frac{x}{2} + \frac{-y}{2\sqrt{3}} \right) \quad f_2 = \sin 2\pi \left( \frac{x}{2} + \frac{y}{2\sqrt{3}} \right) \quad f_3 = \sin 2\pi \left( \frac{y}{\sqrt{3}} \right), \quad (15)$$

with wavevector of length  $\frac{\sqrt{3}}{2}$  the fundamental. In each case, we have chosen the Fourier modes with the shortest wavevectors, as these are easiest to identify in an experimental Fourier transform.

The images of the Fourier transform of pattern (c) in [7] show that the mode created in the instability contains wavevectors that are a factor of 2 shorter than the shortest in the basic hexagonal pattern, which is consistent with representation 10 but not 12. In this way, information about the power spectrum of the pattern is necessary to supplement the arguments based entirely on symmetries and to distinguish between the two choices.

## 5. Normal forms

Using the functions specified above as a basis for representations 7 and 10, the matrices that generate the two relevant representations are, for representation 7:

$$R_{\kappa_x} = I_2, \quad R_\rho = \begin{bmatrix} 1 & 0 \\ 0 & -1 \end{bmatrix}, \quad R_{\tau_1} = \begin{bmatrix} -\frac{1}{2} & \frac{\sqrt{3}}{2} \\ -\frac{\sqrt{3}}{2} & -\frac{1}{2} \end{bmatrix}, \quad R_{\tau_2} = R_{\tau_1}^2, \quad R_{\tau_T} = -I_2, \quad (16)$$

where  $I_n$  is the  $n \times n$  identity matrix; and for representation 10:

$$R_{\kappa_x} = \begin{bmatrix} 0 & 1 & 0 \\ 1 & 0 & 0 \\ 0 & 0 & -1 \end{bmatrix}, \quad R_\rho = \begin{bmatrix} 0 & 0 & -1 \\ 1 & 0 & 0 \\ 0 & 1 & 0 \end{bmatrix}, \quad (17)$$

$$R_{\tau_1} = \begin{bmatrix} -1 & 0 & 0 \\ 0 & 1 & 0 \\ 0 & 0 & -1 \end{bmatrix}, \quad R_{\tau_2} = \begin{bmatrix} -1 & 0 & 0 \\ 0 & -1 & 0 \\ 0 & 0 & 1 \end{bmatrix}, \quad R_{\tau_T} = -I_3. \quad (18)$$

The perturbation amplitude at time  $j + 1$  times the forcing period, given the perturbation at time  $j$ , is given by  $\mathbf{a}_{j+1} = \mathbf{f}(\mathbf{a}_j)$ , where the equivariance condition amounts to  $R_\gamma \mathbf{f}(\mathbf{a}) = \mathbf{f}(R_\gamma \mathbf{a})$  for all  $\gamma \in \Gamma$ . Using this, we can determine the relevant normal form associated with these two representations:

$$z_{j+1} = -(1 + \mu)z_j + P|z_j|^2 z_j + Q|z_j|^4 z_j + R\bar{z}^5 \quad (19)$$

for representation 7 (truncated at quintic order), where the two amplitudes of  $f_1$  and  $f_2$  in (12–13) are the real and imaginary parts of  $z$ , and  $P$ ,  $Q$  and  $R$  are real constants. For representation 10 we truncate at cubic order and obtain:

$$a_{j+1} = -(1 + \mu)a_j + Pa_j^3 + Q(a_j^2 + b_j^2 + c_j^2)a_j, \quad (20)$$

$$b_{j+1} = -(1 + \mu)b_j + Pb_j^3 + Q(a_j^2 + b_j^2 + c_j^2)b_j, \quad (21)$$

$$c_{j+1} = -(1 + \mu)c_j + Pc_j^3 + Q(a_j^2 + b_j^2 + c_j^2)c_j, \quad (22)$$

where  $P$  and  $Q$  are (different) real constants. In these two sets of equations,  $\mu$  represents the bifurcation parameter. The  $-1$  Floquet multipliers at  $\mu = 0$  arise because these are subharmonic bifurcations. In representation 7, equivariance with respect to  $R_{\tau T} = -I_2$  is a normal form symmetry, so even terms up to any order can be removed from (19) by coordinate transformations [9]. With representation 10, the matrix  $-I_3 = R_\rho^3$  appears as a spatial symmetry, so the normal form symmetry is in fact exact, and every solution branch has the spatio-temporal symmetry  $\tau_T \rho^3$ , a rotation by  $180^\circ$  followed by time-translation by one period.

The patterns are neutrally stable with respect to translations in the two horizontal directions, and so also have two Floquet multipliers equal to 1 associated with translation modes. We have neglected these as all the patterns we find are pinned by reflection symmetries that prohibit drifting.

The final stages are to determine the solutions that are created in each of these bifurcations, their symmetry and stability properties, and to compare these with experimental observations.

The first normal form (19) generically has two types of period-two points, found by solving  $f(z) = -z$ :

$$z_a = \sqrt{\frac{\mu}{P} - 2\mu^2 \frac{Q+R}{P^3}}, \quad z_b = i \sqrt{\frac{\mu}{P} - 2\mu^2 \frac{Q-R}{P^3}}. \quad (23)$$

The first of these has exactly the symmetry group  $\Sigma_a$  of pattern (a), with no spatio-temporal symmetries, while the second has exactly the spatial symmetry group  $\Sigma_b$  of pattern (b), as well as spatio-temporal symmetries generated by  $\rho \tau_T$ . Reconstructions of these two are shown in figure 4(a) for pattern (a) and figure 4(b,c) for pattern (b), using the Fourier functions from above. Linearising the normal form about these two period-two points readily yields stability information: if  $P > 0$ , then both patterns are supercritical but only one is stable, while if  $P < 0$ , both are subcritical and neither is stable.

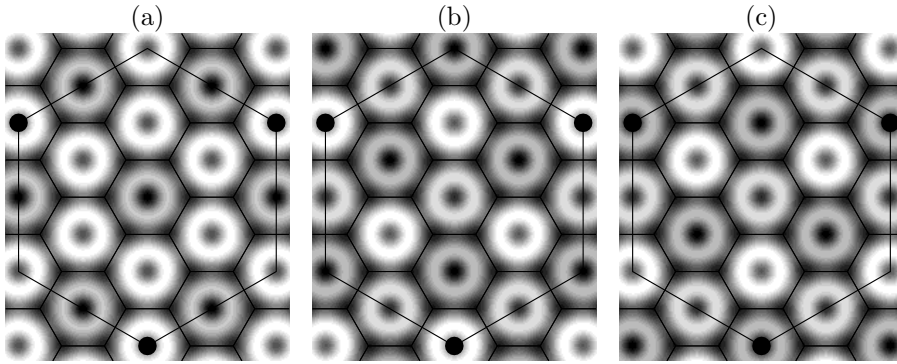


FIGURE 4. Reconstructed patterns from the two solutions that arise in representation 7, using the Fourier functions (12–13) added to a function of the form of (11). (a) has the spatial symmetries of pattern (a) and no spatio-temporal symmetries (cf. 2a,d); (b) has the symmetry properties of pattern (b) (c is one period  $T$  later; cf. figure 2b,e,g)

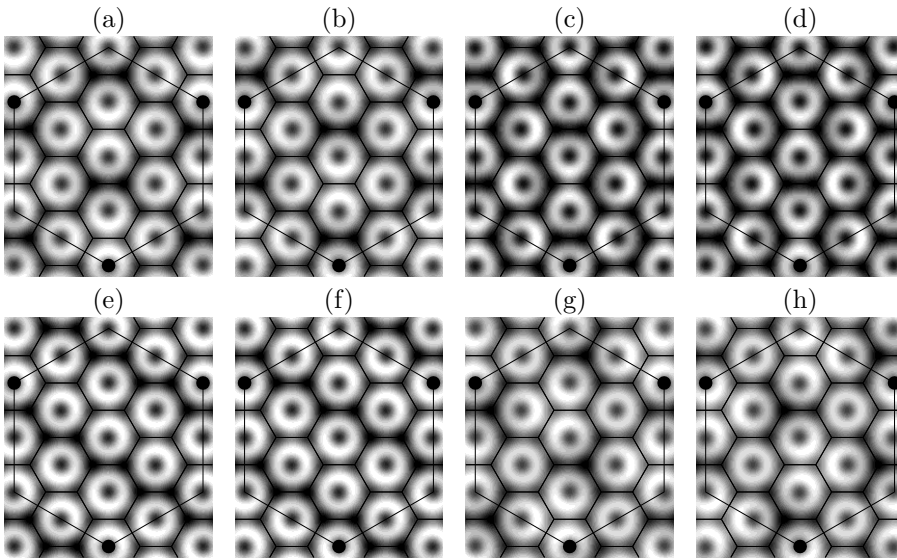


FIGURE 5. Reconstructed patterns from irreps 10 and 12: (a,b) 10:  $(a, b, c) = (1, 1, 0)$  (cf. figure 2c,f,h); (c,d) 12: same amplitudes and same symmetries as (a,b); (e,f) 10:  $(a, b, c) = (1, 0, 0)$ ; (g,h) 10:  $(a, b, c) = (1, 1, 1)$ .

The second normal form (20–22) generically has three types of period-two points  $(a, b, c)$ :

$$\sqrt{\frac{\mu}{P+Q}} \begin{pmatrix} 1 \\ 0 \\ 0 \end{pmatrix}, \quad \sqrt{\frac{\mu}{P+2Q}} \begin{pmatrix} 1 \\ 1 \\ 0 \end{pmatrix}, \quad \sqrt{\frac{\mu}{P+3Q}} \begin{pmatrix} 1 \\ 1 \\ 1 \end{pmatrix}. \quad (24)$$

The middle branch has the spatio-temporal symmetries of pattern (c), with 12 elements in the spatial part of the symmetry group ( $\Sigma_c = \langle \kappa_x, \kappa_y \tau_2, \tau_1^2 \rangle$ ). Figure 5(a,b) illustrates this pattern (cf. figure 2c,f,h). For comparison, the pattern that would have been obtained with modes from representation 12 is in figure 5(c,d): the symmetry group is the same, but the appearance of the pattern does not match the experimental observation. The first branch has a 24 element spatial symmetry group  $\langle \rho^3 \tau_1, \kappa_x \rho \tau_1^5 \tau_2, \tau_1^2 \rangle$  (figure 5e,f), and the third branch has an 18 element group  $\langle \kappa_y \tau_2, \kappa_x \rho^5, \tau_1^2 \rangle$  (figure 5g,h). The three patterns also have the spatio-temporal symmetry  $\rho^3 \tau_T$  (since  $R_\rho^3 = -I_3$ ), so  $\rho^3$  will appear in the symmetry group of the time-average of each of the patterns, as discussed in [1].

The first branch has Floquet multipliers  $-1 + 2\mu$  and  $-1 - \frac{P}{P+Q}\mu$  (twice); the second branch  $-1 + 2\mu$ ,  $-1 - \frac{P}{P+2Q}\mu$  and  $-1 + \frac{2P}{P+2Q}\mu$ ; and the third branch  $-1 + 2\mu$  and  $-1 + \frac{2P}{P+3Q}\mu$  (twice). As a result, if  $P + Q > 0$  and  $P + 3Q > 0$ , then all branches bifurcate supercritically, and either the first branch will be stable (when  $P < 0$ ) or the last will be stable (when  $P > 0$ ). If any branch bifurcates subcritically, none are stable. The middle branch, which is the one corresponding to the experimentally observed pattern (c), is always unstable at onset.

## 6. Discussion

Using the symmetry-based approach of Tse *et al.* [1], we have analysed three experimentally observed spatial period-multiplying transitions from an initial hexagonal pattern. The three patterns illustrate three situations that can arise in this kind of analysis. Pattern (a) was straight-forward, in that a single representation of  $\Gamma$  had a one-dimensional space fixed by the spatial symmetry group of the pattern. The existence of a solution branch of the form of pattern (b) could also be inferred using the Equivariant Branching Lemma, though in this case it was necessary to include the temporal symmetry associated with period-doubling bifurcation. Specifically, the spatial symmetries selected a two-dimensional fixed point space which was further reduced to a one-dimensional fixed point space when spatio-temporal symmetries were taken into account. Experimentally, these two patterns were found for the same fluid parameters and same  $2\omega : 3\omega$  forcing function but for different frequencies  $\omega$ :  $\omega = 25$  Hz for (a) and  $\omega = 35$  Hz for (b). This suggests that the transition between these patterns, which arise for instabilities associated with the same representation, might be observed by tuning the frequency  $\omega$ .

Pattern (c), on the other hand, had a spatial symmetry group that fixed one-dimensional subspaces in two different representations, and we appealed to

the measured power spectrum of the pattern to choose between the two possibilities. In this situation, symmetry considerations alone were not enough. Similar situations arise in other bifurcation problems, for example, knowing that a stable axisymmetric pattern is found in a spherically symmetric bifurcation problem does not provide enough information to determine which is the relevant representation.

The experimentally observed transition between hexagons and pattern (c) occurs by means of a propagating front that separates domains of hexagons and the secondary pattern. The front is initiated at the lateral boundaries of the system and emanates radially inward. There is little if any hysteresis, and the reverse transition also occurs via the same scenario. The occurrence of a front in this transition suggests bistability of the hexagonal pattern and pattern (c). This is certainly consistent with the theoretical prediction that pattern (c) is unstable at small amplitude, that is, at onset. However, we have not explored the possible stabilization mechanisms for pattern (c).

It is worth emphasizing that an understanding of group representation theory is useful in classifying and analysing secondary instabilities of patterns, not only in the Faraday wave experiment as described here, but also in convection and other pattern formation problems (see [10]). It is also worth mentioning that the examples studied here indicate that spatio-temporal symmetries readily arise in secondary subharmonic instabilities, and that careful experimental characterization of these, either by still images taken one forcing period apart or by time-averaging over two forcing periods, can be helpful. Subsequent instabilities of patterns that have spatio-temporal symmetries can be analysed using methods described in [11, 12].

The approach outlined in [1] and here is useful for taking an experimental observation of a secondary transition and casting it into its equivariant bifurcation theory context, but it does not predict which transitions should be expected in an experiment. However, in these two-frequency Faraday wave experiments, three-wave interactions of the type described in [13] may select a third wavevector that could appear in the secondary transition. Each of the representations in the problem under consideration is associated with a set of wavevectors, providing a possible mechanism for selecting between possibilities.

**Acknowledgements.** This paper builds on earlier published results obtained with Dawn Tse, Rebecca Hoyle and Hagai Arbell. AMR is grateful for support from the EPSRC. The research of MS is supported in part by NSF grant DMS-9972059 and NASA grant NAG3-2364. JF is grateful for support from the Israel Academy of Science (grant 203/99).

## References

- [1] Tse, D.P., Rucklidge, A.M., Hoyle, R.B. & Silber, M., *Spatial period-multiplying instabilities of hexagonal Faraday waves*, *Physica*, **146D** (2000), 367–387.
- [2] Edwards, W.S. & Fauve, S., *Patterns and quasi-patterns in the Faraday experiment*, *J. Fluid Mech.*, **278** (1994), 123–148.

- [3] Kudrolli, A. & Gollub, J.P., *Patterns and spatiotemporal chaos in parametrically forced surface waves: a systematic survey at large aspect ratio*, *Physica*, **97D** (1996), 133–154.
- [4] Müller, H.W., Friedrich, R. & Papathanassiou, D. (1998) Theoretical and experimental investigations of the Faraday instability. In *Evolution of Spontaneous Structures in Dissipative Continuous Systems* (ed. F.H. Busse & S.C. Müller), pp. 230–265. Springer: Berlin
- [5] Golubitsky, M., Stewart, I. & Schaeffer, D.G. (1988) *Singularities and Groups in Bifurcation Theory. Volume II*. Springer: New York.
- [6] Kudrolli, A., Pier, B. & Gollub, J.P., *Superlattice patterns in surface waves*, *Physica*, **123D** (1998), 99–111.
- [7] Arbell, H. & Fineberg, J., *Spatial and temporal dynamics of two interacting modes in parametrically driven surface waves*, *Phys. Rev. Lett.*, **81** (1998), 4384–4387.
- [8] Lioubashevski, O., Arbell, H. & Fineberg, J., *Dissipative solitary states in driven surface waves*, *Phys. Rev. Lett.*, **76** (1996), 3959–3962.
- [9] Elphick, C., Tirapegui, E., Brachet, M.E., Coulet, P. & Iooss, G., *A simple global characterization for normal forms of singular vector fields*, *Physica*, **29D** (1987), 95–127.
- [10] Rucklidge, A.M., Weiss, N.O., Brownjohn, D.P., Matthews, P.C. & Proctor, M.R.E., *Compressible magnetoconvection in three dimensions: pattern formation in a strongly stratified layer*, *J. Fluid Mech.*, **419** (2000), 283–323.
- [11] Rucklidge, A.M. & Silber, M., *Bifurcations of periodic orbits with spatio-temporal symmetries*, *Nonlinearity*, **11** (1998), 1435–1455.
- [12] Lamb, J.S.W. & Melbourne, I. (1999) Bifurcation from periodic solutions with spatiotemporal symmetry. In *Pattern Formation in Continuous and Coupled Systems* (ed. M. Golubitsky, D. Luss & S.H. Strogatz), pp. 175–191. Springer: New York
- [13] Silber, M., Topaz, C.M. & Skeldon, A.C., *Two-frequency forced Faraday waves: weakly damped modes and patterns selection*, *Physica*, **143D** (2000), 205–225.

Department of Applied Mathematics,  
University of Leeds, Leeds LS2 9JT UK  
*E-mail address:* A.M.Rucklidge@leeds.ac.uk

Department of Engineering Sciences and Applied Mathematics,  
Northwestern University, Evanston IL 60208 USA  
*E-mail address:* m-silber@northwestern.edu

The Racah Institute of Physics,  
The Hebrew University of Jerusalem,  
Givat Ram, Jerusalem 91904 Israel  
*E-mail address:* jay@vms.huji.ac.il